An investigation into the longitudinal dynamics and control of a flapping wing micro air vehicle at hovering flight

K. Loh, M. Cook, P. Thomasson
Flight Dynamics Group, College of Aeronautics
Cranfield University, UK

ABSTRACT

This paper describes the research into the flight dynamics modelling and flight control of a flapping wing micro aerial vehicle (MAV). The equations of motion based on a multi-body representation of the vehicle and the flapping wings were derived and form the basis for the simulation program, which was developed using MATLAB and SIMULINK. The aerodynamic forces were obtained through experimental methods and form the basis for the aerodynamic model.

The hovering and low speed flight of the MAV was investigated using a SIMULINK simulation model. Various flight control concepts, inspired by observation of insect and bird flight, were investigated in some detail. The concepts include the control of flap frequency, flap and pitch phasing (wing beat kinematics) and shift in centre of gravity position. The paper concludes with a comparison of the control concepts and their feasibility for a practical vehicle application.

NOMENCLATURE

$\mathbf{a}$	vector $[a_x \ a_y \ a_z]^T$
$\mathbf{a}^\times$	skew symmetric form of vector $\mathbf{a}$ $\begin{bmatrix} 0 & -a_z & a_y \\ a_z & 0 & -a_x \\ -a_y & a_x & 0 \end{bmatrix}$
$\mathbf{A}$	3×3 matrix
$\mathbf{b_i}$	position vector of wing attachment from origin of fuselage reference system
$\mathbf{d_i}$	position vector of centre of gravity of R_i from origin of body reference system
$\mathbf{C_{ij}}$	direction cosine matrix from coordinate system j to coordinate system i
C_{xi}, C_{yi}, C_{zi}	aerodynamic force coefficients in the x-, y- and z-directions of the co-ordinate system i
$\mathbf{f}$	column vector of external forces acting on a body
$F_{x,aero}$, $F_{y,aero}$, $F_{z,aero}$	aerodynamic forces in the x-, y- and z-directions
$^{\mathbf{i}}\mathbf{F}$	column vector of forces in the co-ordinate system I
g	acceleration due to gravity in inertial reference system $[0\ 0\ g]^T$
K, k	gain
$\mathbf{l_{ac}}$	position vector of wing aerodynamic centre from origin of wing reference system
m	mass of fuselage
M_{aero}	aerodynamic moment
$\mathbf{M}$	generalised mass matrix
n	flap frequency
$\mathbf{P_1}$	position vector of origin of fuselage reference system in the inertial reference system
q_b	fuselage pitch rate
r	span of each wing from root to tip
R_i	i-th body in multi-body system
S_{wing}	wing reference area
s	Laplace variable
$u_b\ v_b\ w_b$	fuselage velocity components in fuselage reference system
$\mathbf{v_o}$	velocity vector of fuselage $[u_b \ v_b \ w_b]^T$
$\mathbf{V}$	state vector $[\mathbf{v_o}\ \boldsymbol{\omega_1}\ \boldsymbol{\omega_{p2}}\ \boldsymbol{\omega_{p3}}]^\mathbf{T}$
V_f	flap velocity
x_i, y_i, z_i	Cartesian co-ordinates of the i-th axes system

Greek symbols

$\bar{\alpha}, \hat{\alpha}, \dot{\alpha}, \ddot{\alpha}$	mean, amplitude, first time derivative and second time derivative of angle α
χ	pitch degree of freedom of wing
δ	flap degree of freedom of wing
κ	stroke plane angle of wing
ρ	density of air
φ	phase lead between pitch and flap degrees of freedom of wing
$\boldsymbol{\Phi}$	wing attitude vector $[\chi \ \delta \ 0]^\mathbf{T}$
ϕ, θ, ψ	roll, pitch and azimuth of fuselage

Paper No. 2817. Manuscript received 2 December 2002, accepted 6 June 2003.

ϑ	vector of Euler angles of fuselage $[\phi\ \theta\ \psi]_T$
$\omega_{pi} = \omega_i - \omega_1$	column vector of relative angular velocity of a wing with respect to fuselage
ω_i	column vector of angular velocity of Ri

Subscript

aero	aerodynamic component
E	Euler
b	fuselage
p	port
s	starboard
0	inertial frame
1	fuselage
2,3	port and starboard wing actuator motor
4,5	port and starboard wing

1.0 INTRODUCTION

Flapping wing flight by insects, birds and bats has long been the interest of zoologists and entomologists. The aeronautical community in the days before the Wright brothers had experimented with this form of flight but its complexity and the lack of understanding made meaningful progress impossible. Instead, 'simpler' flight was eventually achieved in the forms of the fixed wing aircraft and the rather more complicated rotary wing aircraft.

Lately, following the rapid and substantial progress in micro-electro-mechanical systems (MEMS), flapping wing flight has again aroused the interest of aeronautical engineers. This can be seen in many research projects carried out by traditional aeronautical departments of universities and research institutes. The main source of this interest is the new requirement for micro air vehicles (MAVs) identified by Defense Advanced Research Projects Agency (DARPA) in the United States of America. These MAVs are to be used in surveillance and intelligence gathering missions. Such air vehicles fly at very low Reynolds numbers (low flight velocity and small size as the name implies). Conventional fixed wing designs must fly at high speeds to generate sufficient lift, making the aircraft less agile, a requirement much needed for operation in enclosed spaces. Also, at such low Reynolds number, the maximum lift-to-drag ratio of most current aerofoils is reduced significantly[1] such that high drag must be overcome. In order to reduce power requirement, new aerofoils have to be developed.

Zoologists and entomologists have for some time recognised that birds and insects make use of unsteady aerodynamics[2,3] to generate additional lift when they flap their wings in flight, combining the mechanisms of delayed stall[4], wake capture and rotational circulation[5]. If mastered, flapping wings could provide the combined propulsion and weight support mechanism for the micro air vehicle. The low aerodynamic power per unit mass requirement of flapping flight of less than 70W/kg[6-8] is less than half the requirement for fixed wing aircraft as quoted by Zbikowski[9] and coupled with the manoeuvrability exhibited by insects, bats and birds makes it an attractive alternative.

These considerations, coupled with the more sophisticated tools made available by developments in aeronautical engineering, allow researchers to revisit many of the problems asscociated with flapping wing flight. DeLaurier has achieved sustained and controlled flight with his 10ft span ornithopter[10]. Similarly, AeroVironment developed a micro-air vehicle named Microbat with a 15·2cm wingspan, weighing 10g and capable of an 18-second flight with wings flapping at 20Hz[11].

Research on flapping wing flight is multi-disciplinary and zoologists, entomologists and aeronautical engineers are contributing to the knowledge and expertise. Typical research encompasses the development of a milli-scaled reciprocating chemical muscle in Georgia Technological Research Institute[12]. Others have carried out studies of the wing beat kinematics of insects[13-16] and birds[17,18], computational fluid dynamics studies[19-21] and flow visualisation of flapping wings[22]. Others have attempted to attach force-measuring devices to living animals[23] in an attempt to extract information on the time dependent loads.

Various experimenters have also attempted to measure forces generated by mechanically flapped wings in wind tunnels[24,25], water tunnels[26] and oil tanks[27].

Loh[28] has developed a mechanical flapper to measure the aerodynamic forces experienced by a wing performing sinusoidal motion in its pitch and flap degrees of freedom. The tests carried out also investigated the effects of variation in the phase angle between the two degrees of freedom on the magnitude and direction of the wing aerodynamic forces.

The flight dynamics and control of a vehicle employing such a flight mode has, until recently, received very little attention. Although qualitative accounts on the stability and control[29] and papers based on the observation[30] of insect flight were available, the only document on the mathematical modelling and simulation at the start of the current research in 1999 was the thesis by Rashid[31] who studied the open-loop flight dynamics of the ornithopter designed by DeLaurier and Harris. However, this vacuum has been filled by the flush of recent publications on the subject[32-34] on the control of the micromechanical flying insect (MFI) currently in development at the University of California, Berkeley (UC Berkeley). The aeronautics community has realised that when the stability and control 'is worked out the age of flying machines will have arrived, for all other difficulties are of minor importance' — Wilbur Wright, 1901[35].

The current paper describes the research into three different control concepts using classical control theory for the stabilisation and control of a virtual flapping wing micro air vehicle, which weighs about 4g and flaps with a frequency of 40Hz. The control concepts studied here differ from that of the MFI of UC Berkeley. Instead of continuously adjusting the wing parameters within a flap cycle, the wings of our vehicle flap with unchanged parameters within the flap cycle. Variation of parameters only occurs at the end of a flap cycle. This allows a slower controller to be implemented, placing a less stringent requirement on the controller design.

2.0 CANDIDATE MAV DESIGN

The subject of this research is a notional virtual flapping wing micro air vehicle as shown in Fig. 1. While the authors acknowledge the limitations of current technology, it is assumed that the technology will eventually become available for a prototype to be manufactured to its specifications.

The vehicle comprises a cigar shaped fuselage, which houses all the essential equipment. Figure 2 shows a possible arrangement of the equipment. The payload, presumably a micro video camera or some other micro sensors and transmitter, is assumed to be carried at the forward section in order to have unobstructed view. The locations of the power, transmission and fuel or battery units, which are expected to form the bulk of the mass of the vehicle, have a significant effect on the pitch inertia of the vehicle. A compromise has to be made between responsiveness in pitch of the vehicle and its effect on the 'picture' quality transmitted back to the base. In order to increase the pitch inertia of the fuselage, the power transmission actuators are placed near the wing attachment points, while the power and fuel/battery units are located at the aft sections. The flight control computer is assumed to be located between the fuel/battery compartment and the transmission units.

As shown in Fig. 3, each of the two wings of the vehicle has two degrees of freedom, namely in flap and pitch. The stroke plane, defined by the wing attachment point and the locus of the wing tip, can further be rotated about an axis lying in the fuselage vertical plane ($P_1 x_1 y_1$ plane). The stroke plane angle is the angle between

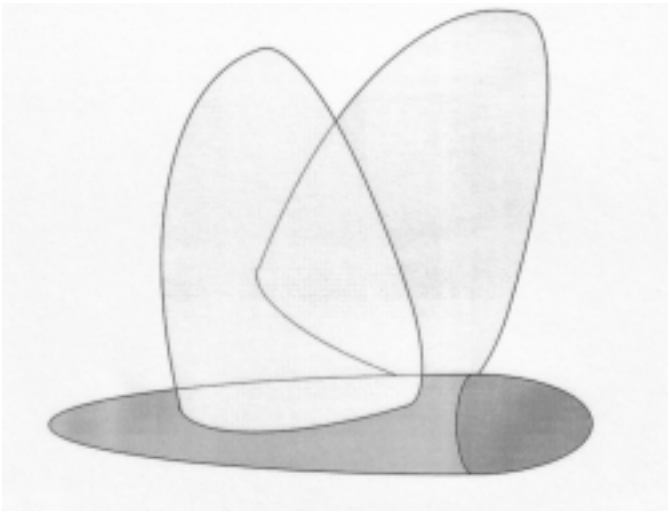

Figure 1. Artist impression of the MAV.

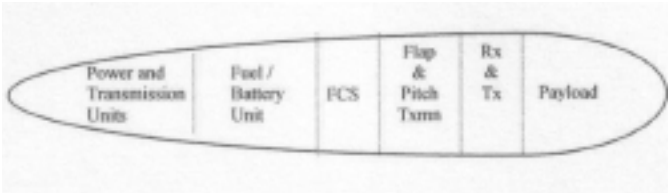

Figure 2. General layout of essential equipment in fuselage of FMAV.

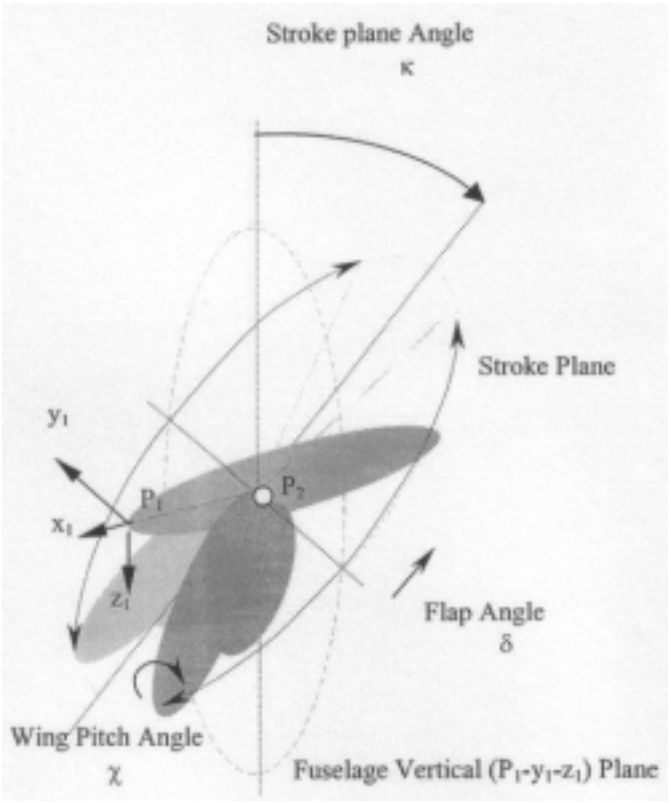

Figure 3. Illustration of wing degrees of freedom.

Table 1
Mass breakdown estimation based on first generation Black Widow

Elements	% of total mass of FMAV	% of total mass of Black Widow
Fuselage and structure	14	17
Wings	5	
Power units	25	62
Transmission units	25	
Fuel units	10	
Flight control computer	9	9
Payload	10	12
Transmitter	2	

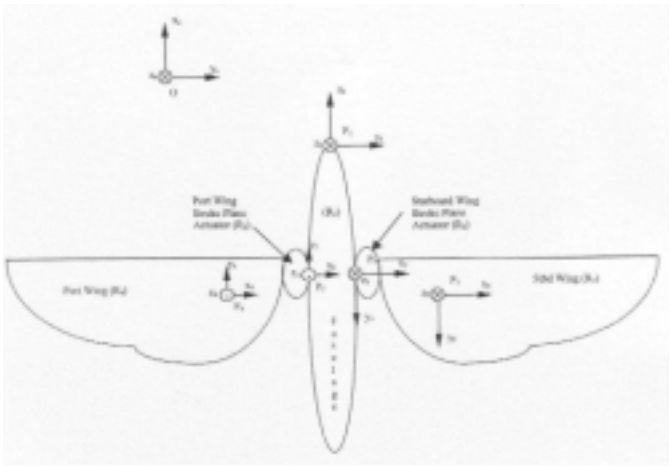

Figure 4. Definitions of co-ordinate systems for the MAV model.

the *y*-*z* plane of the fuselage and the stroke plane. It is assumed that one motor independently drives one of the two degrees of freedom of each wing and a third drives the stroke plane angle.

The mass and inertia properties of the vehicle are estimated based on the data found in Grasmeyer and Keenon (2001) for the first generation Black Widow MAV weighing 56g. This is given in Table 1.

3.0 THE MATHEMATICAL MODEL

3.1 Definition of axes systems and direction cosine matrices

The MAV can be modelled by linking the fuselage (R_1), two stroke plane actuators (R_2 and R_3) and two wings (R_4 and R_5) as shown in Fig. 4. Each of the five individual bodies R_i (i = 1 to 5) has a right-handed orthogonal axes system ($P_i x_i y_i z_i$) affixed to it at P_i.

In addition, the spatial north-east-down (NED) reference system $Ox_0 y_0 z_0$ is defined with the axes pointing towards the north (Ox_0), east (Oy_0) directions and towards the centre of the Earth (Oz_0). This is a Galilean system, ie it is non-rotational and fixed in space.

The fuselage has six degrees of freedom defined by its position $\mathbf{P_1} = [x_b\ y_b\ z_b]^T$ and its Euler orientation in bank, pitch and azimuth $\vartheta = [\phi\ \theta\ \psi]^T$. Each of the two stroke plane actuators has a single degree of freedom (stroke plane angles κ_p and κ_s). Each wing has two degrees of freedom in pitch (χ) and flap (δ). The orientation of the

Table 2
Definition of signs for variables

Variable	
X_0	Vehicle CG is north of the origin of the NED system
Y_0	Vehicle CG is east of the origin of the NED system
Z_0	Vehicle CG is below of the origin of the NED system
X_1	The referred point is forward of the origin of the fuselage axes system
Y_1	The referred point is on the port side of the origin of the fuselage axes system
Z_1	The referred point is below of the origin of the fuselage axes system
ϕ	If both wings have the same orientation, the vehicle is banked with port wing higher than the starboard wing
θ	The vehicle has a nose up pitch attitude
ψ	The vehicle is yawed clockwise about the down axes of the NED system
κ_p, κ_s	The stroke plane is tilted from the vertical such that with the wing at the extreme upstroke position, it is behind the wing attachment point P_2 or P_3
δ_p, δ_s	The wing is flapped with the wings above the wing level position
χ_p, χ_s	The wing is pitched with the leading edge up and trailing edge down

port wing is defined by $\mathbf{\Phi p} = [\kappa_p\ \delta_p\ \chi_p]^T$ and that of the starboard wing by $\mathbf{\Phi_s} = [\kappa_s\ \delta_s\ \chi_s]^T$.

The orientations for the NED and fuselage axes-systems are consistent with aircraft representation. The orientations for axes systems of the wings and the stroke plane actuators are determined by the need for consistent definitions for the stroke plane angle (κ), flap (δ) and pitch (χ) angles about the axes of the wing co-ordinate systems for both wings. Table 2 shows the meaning of a positive value in each of the variables in the above notation.

The transformation of a vector from the *i*-th axes system ($^i\mathbf{a}$) to the *j*-th axes system ($^j\mathbf{a}$) is governed by the following equation

$$^j\mathbf{a} = \mathbf{C_{ji}}\ ^i\mathbf{a} \qquad \ldots\ (1)$$

where $\mathbf{C_{ji}}$ is the direction cosine matrix.

3.2 The equations of motion of the multi-body system

The equations of motion are developed by considering the linear and angular momentum of the system of bodies and the externally applied forces and moments in the Newton-Euler formulation. This gives rise to a system of 18 equations, which can be assembled as

$$\dot{\mathbf{V}} = \mathbf{M}^{-1}\left(\mathbf{F} + \mathbf{F_{dyn}}\right) \qquad \ldots\ (2)$$

The vector of state derivatives is $\dot{\mathbf{V}} = \left[\dot{\mathbf{v}}_0\ \dot{\mathbf{u}}_1\ \dot{\mathbf{u}}_{p2}\ \dot{\mathbf{u}}_{p3}\ \dot{\mathbf{u}}_{p4}\ \dot{\mathbf{u}}_{p5}\right]^T$. The matrix $\mathbf{M^{-1}}$ is the inverse of the generalised mass matrix containing the masses and inertias of the fuselage and wings. $\mathbf{F}$ is the vector of applied forces and torques due to the aerodynamics of the wings, gravity and actuator motors. $\mathbf{F_{dyn}}$ is the vector of dynamic forces and torques due to the motion of the bodies. They can be classified as inertial, centrifugal and Coriolis forces and moments, and moments due to gyroscopic precession.

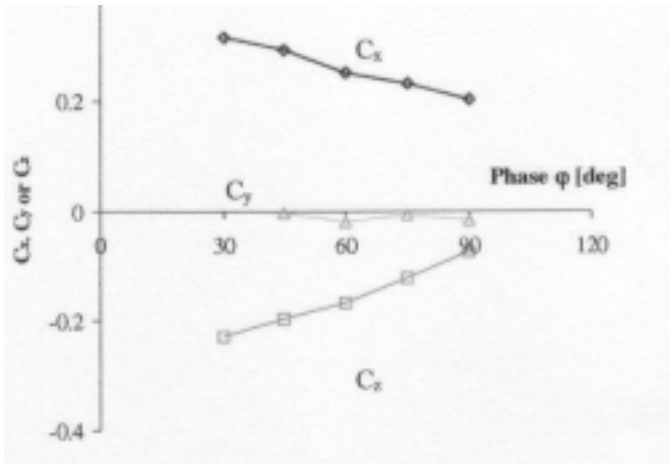

Figure 5. Time averaged force coefficients for aerodynamic model.

The solution to Equation (2) was time-consuming as the time step must be smaller than 50 steps per flap cycle or 5 milliseconds in order to achieve a good representation of the flap dynamics. Observation of the solution of the full order equations of motion showed that the oscillations are about a mean value that cancel out over a flap cycle and the predominant forces transmitted from the wings to the fuselage are the aerodynamic and centrifugal forces. The centrifugal forces are practically unaffected by the pitching of the wings.

Hence, by averaging each state over a flap cycle, the effects of the time-averaged dynamic forces are retained and the computational time is vastly reduced. By so doing, the problem of a stiff system created by the low frequency fuselage response and the high frequency of the flapping wing were also avoided. The time varying state ω_{p4} and ω_{p5} and their related terms can then be removed if they occur in odd powers in Equation (2). The state derivative is reduced to $\dot{\mathbf{V}} = \left[\dot{\mathbf{v}}_0\ \ \dot{\mathbf{u}}_1\ \ \dot{\mathbf{u}}_{p2}\ \ \dot{\mathbf{u}}_{p3}\right]$ and Equation (2) is of order 12.

The state derivatives can be integrated to obtain the states of the fuselage and the wings. These can then be transformed to obtain the Euler rates (Equations (3) to (5)) and integrated once more to obtain the wing orientation Φ, vehicle position $\mathbf{P_1}$ and vehicle orientation $\boldsymbol{\vartheta}$.

$$\dot{\vartheta} = \mathbf{C}_{\vartheta\omega}\dot{\mathbf{u}}_1 \qquad \ldots\ (3)$$

$$\dot{\Phi}_i = \mathbf{C}_{\Phi\omega}\dot{\mathbf{u}}_{pi} \qquad \ldots\ (4)$$

$$\dot{\mathbf{P}}_1 = \mathbf{C}_{01}\mathbf{v}_o \qquad \ldots\ (5)$$

3.3 The aerodynamic model

The aerodynamic contribution is assumed to derive solely from the wings in the present study of low-speed and hovering flight. The effect of the small amplitude vehicle motion on the aerodynamics of the wings is also assumed to be negligible as compared to the high frequency flapping of the wings. Finally, it is further assumed that the change in stroke plane is relatively slow enough for its effects on the wing aerodynamics to be neglected.

The aerodynamic force coefficients were obtained from experiments conducted with the flapper in still air as described in Loh[28]. These time-averaged force coefficients, as functions of the phase angle φ between the flap and pitch degrees of freedom, are shown in Fig. 5. These are then used to compute the aerodynamic forces according to Equation (6)

$$F_{k,aero} = \tfrac{1}{2}\rho V_f^2 S_{wing} C_k \qquad \ldots\ (6)$$

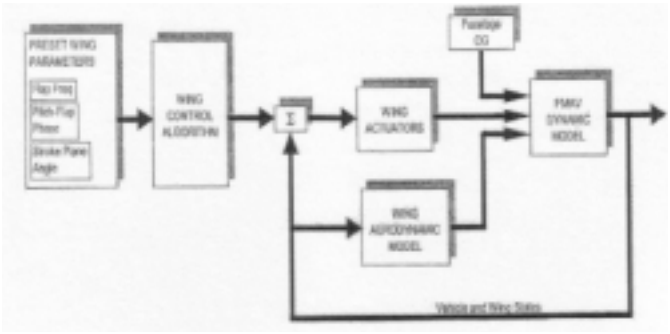

Figure 6. Open loop MAV simulation model.

where k is the axis in question and the nominal flap velocity V_f is given by

$$V_f = \frac{nr\hat{\delta}}{2} \quad \ldots (7)$$

The aerodynamic forces act at the aerodynamic centre of the wing, which is assumed to be at a distance lac from the wing attachment point. This generates an aerodynamic moment M_{aero} at the wing attachment point given by

$$M_{aero} = l_{ac}{}^{x} F_{aero} \quad \ldots (8)$$

where $F_{aero} = [F_{x,\,aero}\ \ F_{y,\,aero}\ \ F_{z,\,aero}]^T$.

4.0 OPEN LOOP SIMULINK MODEL

Figure 6 shows the open loop SIMULINK model of the vehicle. The wing kinematics is prescribed by specifying the flap frequency, the phase between pitch and flap attitudes and the stroke plane angle of each wing. The wings then follow the prescribed sinusoidal motion. The actual and demanded attitude of the wings then form appropriate error signals for the actuator motors, which drive the wings.

The actuator motor torques and the aerodynamic forces and moments experienced by the wings in motion form the input for the equations of motion, which are programmed into the *S*-function called *FMAV_Dynamics*. It computes and outputs the state derivatives according to Equation (1). These are then transformed to the Euler rates and fuselage velocity components according to Equation (3) to Equation (5) and finally integrated to obtain the fuselage position and orientation and wing orientation.

4.1 Longitudinal trim of the vehicle

With the vehicle assumed to be symmetric, setting the roll angle to zero and assuming that both the port and starboard wings execute identical motion, the vehicle can be assumed to be in lateral-directional trim at hover. It is then necessary to trim the vehicle longitudinally before the model can be linearised.

Figure 7 shows the force and moment balance about the pitch axis. Acting on the wing attachment points P_2 and P_3 are the resultant external force and moment. These are due to the motion of the wings (dynamic), gravity, actuator motor and the aerodynamics of the wings. In order for the vehicle to be in equilibrium, the resultant force must generate a moment about the fuselage centre of gravity that counters the resultant moment.

The forces and moment equations for equilibrium can thus be written as

$$\mathbf{d}_i^{\times}\mathbf{C}_{1E}m\mathbf{g} + \sum_{i=2}^{5}\mathbf{b}_i^{\times}\mathbf{C}_{1i}\mathbf{F}_i + \sum_{i=1}^{5}\mathbf{C}_{1i}\mathbf{M}_i = 0 \quad \ldots (9)$$

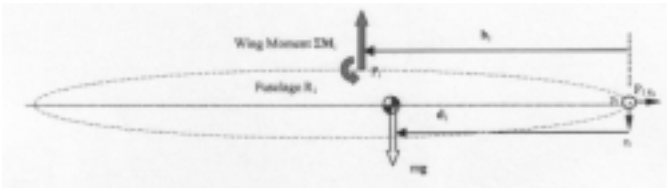

Figure 7. Forces and moments acting on fuselage.

$$\sum_{i=1}^{5}\mathbf{F}_{xi} = 0 \quad \ldots (10)$$

$$\sum_{i=1}^{5}\mathbf{F}_{zi} = 0 \quad \ldots (11)$$

At, or near, equilibrium, assume that the dynamic forces and moments are negligible and thus only gravity and aerodynamic components are significant. As can be expected, the location of the centre of gravity plays a critical role for moment balance.

Equation (10) determines the stroke plane angle κ of the wings. Starting from an initial estimated value of κ_o, the longitudinal acceleration can be found from the simulation and the stroke plane angle can be adjusted iteratively using an appropriate value for the gain K_κ in Equation (12) until the longitudinal acceleration falls within the pre-set tolerance:

$$\hat{\mathrm{e}} = \hat{\mathrm{e}}_o + \Delta = \hat{\mathrm{e}}_o + \hat{\mathrm{e}}_K\ddot{x} \quad \ldots (12)$$

where $\hat{\mathrm{e}}_o = \mathrm{Tan}^{-1}\dfrac{C_{x,aero}}{\left|C_{z,aero}\right|}$

In the trim algorithm used, the mass of the fuselage m_1 and the location of the centre of gravity of the fuselage $\mathbf{d_1}$ from the origin of the fuselage axes system P_1 are allowed to vary as the other parameters in Equation (9) and Equation (10) are fixed. It is further assumed that $\mathbf{d_1} = [\mathbf{d_{1x}}\ 0\ 0]^{\mathbf{T}}$, i.e. the CG only varies longitudinally. We are thus able to determine the trim parameters.

Using the so attained trim parameters, it was found that the vehicle drifts slowly from the trimmed state. This is a manifestation of both the trim routine as well as the vehicle dynamics. The longitudinal, vertical and angular accelerations are iteratively reduced during the trim routine until they are smaller than the pre-set tolerance, but still remain non-zero. This causes the vehicle to accelerate, albeit very slowly. Added to this, the vehicle is neutrally stable because the resultant force vector has to be absolutely vertical in order to maintain the perfect hover. Any tilt in this vector causes the vehicle to accelerate forward, lose altitude and pitch. There is no restoring moment or force in the open loop to return the vehicle to the trim condition, hence the divergence.

Mathematically, this can be seen in the open loop eigenvalues of the linearised model of the vehicle. The model has 20 eigenvalues, 12 from the state equations and eight from the output equations of the simulation model. Out of these 20 eigenvalues, 16 are real at the origin of the *s*-plane and the other four form two conjugate pairs. The real roots at the origin indicate neutrally stable roots of the system and the reasons why the system output drifts slowly. The conjugate roots are the wing actuator motor roots and the vehicle short period pitching mode.

4.2 Pitch stabilisation

In order to stabilise the pitch mode, the eigenvector related to this mode was investigated and found that the main components are pitch rate q_b and the stroke plane angle rates ω_{2x} and ω_{3x}. It is not surprising that fuselage pitch rate feedback is required for stabilisation.

For the control concepts investigated in this paper, one control

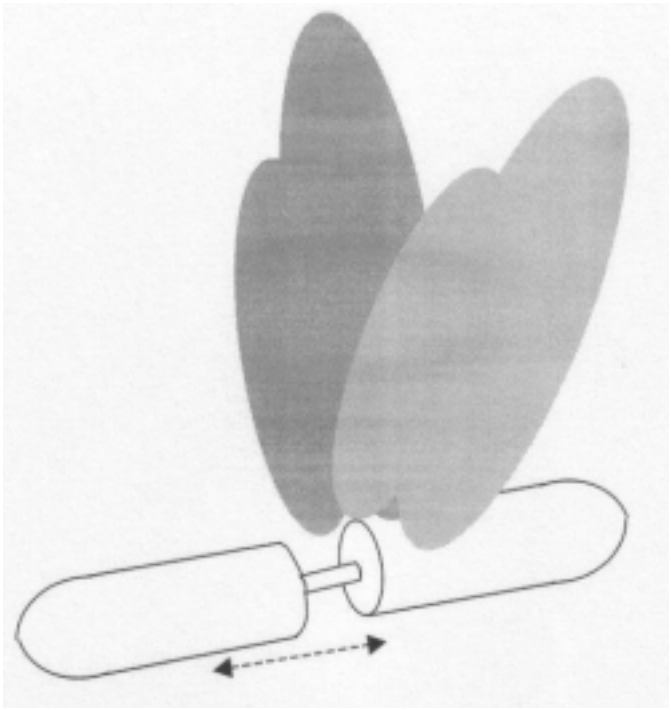

Figure 8(a). Variation through 'sliding' fuselage.

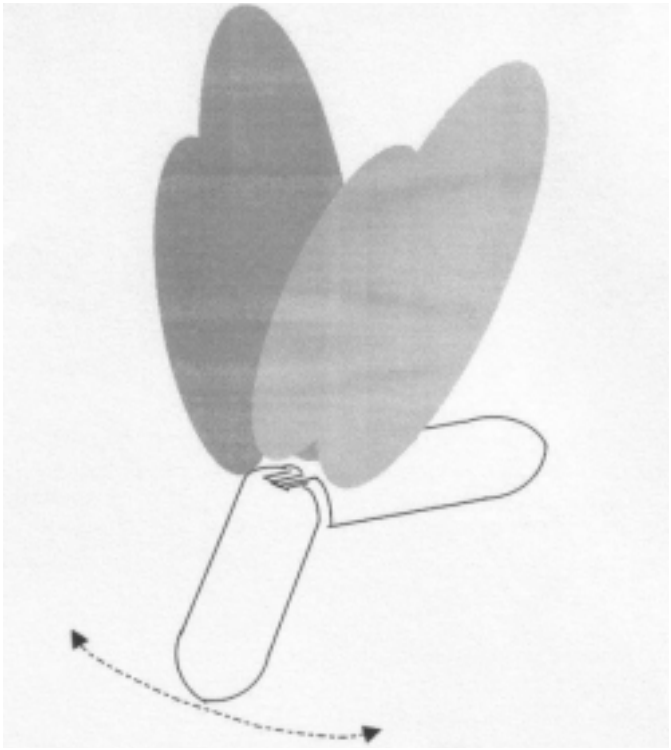

Figure 8(b). CG variation through 'hinged' fuselage.

input is specified for each output to be controlled. Four possible control inputs can be used, namely the stroke plane angle, flap frequency, the phase between the pitch and flap attitudes and the CG location of the fuselage.

Since the phase between the pitch and flap attitudes affects the magnitude of the resultant time-averaged force, it was proposed to use either this, or flap frequency, for force magnitude control, and hence climb rate (w_b) control. As suggested in the trimming of the vehicle, the stroke plane angle is used to control u_b. Thus to control the pitch of the vehicle, positive feedback of pitch rate to the CG location was found to stabilise the vehicle.

This is a mechanism observed in insects and birds at the hover: the abdomen of the insects being brought in and out during the hover, seemingly to balance in pitch. A servo can be used to drive a mass linearly to control the location of the centre of gravity of the fuselage, as shown in Fig. 8(a). Alternatively, the fuselage can be divided into two separate parts hinged at the joint controlled by an actuator motor, as shown in Fig. 8(b).

The linear open loop transfer function for the pitch rate response to perturbation in the centre of gravity location for the vehicle with variable flap frequency is given by the following expression, after the common terms in the numerator and denominator are removed

$$\frac{q_b(s)}{c(s)} = G(s) = \frac{-3,006 \cdot 3\left(s^2 + 220s + 25,000\right)}{s\left(s^2 + 267s + 30,344\right)} \quad \ldots (13)$$

The closed loop characteristic equation with negative feedback is given by $1+kG(s)$, which results in a conjugate pair of roots and a real root whose position determines the exponential rate of decay. An appropriate feedback gain k can be selected using root locus methods to stabilise the system. For example, choosing k_q = –0·016 m/(rad.s^{-1}) provides a satisfactory level of stability.

The experimental results in Fig. 5 suggest that a variation in the phase between the wing pitch and flap can be used to modulate the resultant force magnitude. If this is used instead of the flap frequency, it is found that the feedback gain k_q can be set to –0·05 m/(rad.s^{-1}) to attain pitch stability.

Table 3
Definition of control concepts

Control concept	*X*-Channel	*Z*-Channel
1	Stroke plane tilt	Variation of flap frequency
2	Stroke plane tilt	Variation of phase between pitch and flap degrees of freedom of wings
3	Fuselage tilt through CG shift	Variation of phase between pitch and flap degrees of freedom of wings

5.0 CONTROL CONCEPTS

In the study undertaken by Schenato *et al*[32] at UC Berkely, the control of the MFI using the flap frequency variation as force magnitude modulation and the active control of wing attitude and angle-of-attack to control pitch moment as well as force direction was investigated. Inherently, the wing parameters have to be controlled at frequencies much higher than the flap frequency in order to prevent aliasing of the signals. Flapping at 150Hz may require signals to be sensed, computed and more importantly actuated at frequencies in excess of 7·5kHz, if 50 data points were sensed per flap cycle. This may place an unnecessary demand on the specifications for the miniature servos.

By suggesting that pitch stabilisation be achieved by centre of gravity shift at only a fraction of the nominal flap frequency, the demand for exceptionally fast actuation can be removed. Possible means of achieving this have been described earlier as shown in Figs 8(a) and (b).

In this study, three concepts of position and velocity control for the candidate MAV were investigated based on two alternative methods to

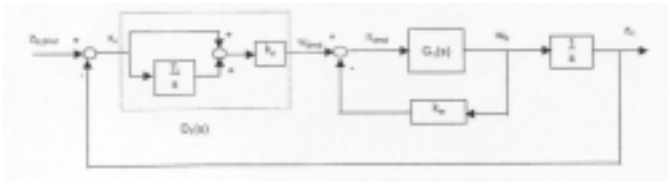

Figure 9. Vertical position demand loop.

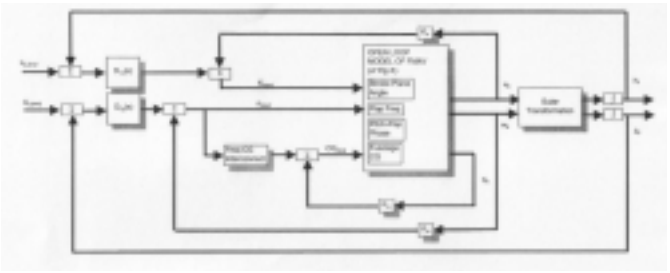

Figure 10. Flight control system for Concept 1.

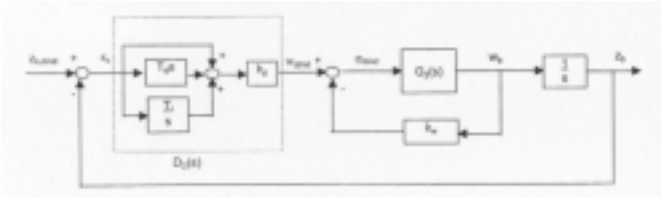

Figure 11. Vertical position demand loop.

control the vertical position (variation of flap frequency or phase between pitch and flap) and two methods to control the horizontal position (stroke plane tilt or fuselage tilt) as summarised in Table 3.

One of the most straightforward means for force modulation is through a change in the flap frequency. However, by maintaining a constant flap frequency and varying the phase between pitch and flap instead, the design of the mechanical parts could be optimised. The energy used to flap the wings at a frequency close to its natural frequency would also be minimised.

Similarly, tilting the stroke plane seems an obvious method to direct the force vector. As an alternative, the stroke plane angle can be limited and the fuselage allowed to pitch instead. The mechanisms to drive the stroke plane can thus be eliminated, allowing for a weight saving, as the servo to shift the fuselage centre of gravity is already necessary to maintain pitch stability.

In the subsequent design of the flight control systems, the gains are selected by determining the damping ratio and natural frequencies based on evaluation of the closed loop characteristic equations, pole placement methods and some degree of empiricism.

5.1 Control Concept 1

In this concept, the flap frequency is varied for vertical axis control (z-channel) while the stroke plane tilt controls the horizontal axis (x-channel). By varying the flap frequency, the moment balance as given in Equation (9) is inadvertently modified. As the perturbation moment is aerodynamic in nature due to the variation in the flapping frequency from n_1 to n_2, simply varying $\mathbf{d}_1$ in the inverse proportion to the ratio of actual and nominal flapping frequency can maintain this moment balance

$$\mathbf{d}_{1(n=n_2)} = \left(\frac{n_2}{n_1}\right)^2 \mathbf{d}_{1(n=n_1)} \qquad \ldots (14)$$

The linear transfer function for the response of the rate of climb w_b to a change in flap frequency is given by

$$G_1(s) = \frac{w_b(s)}{n_{dmd}(s)} = \frac{K_{fw}}{s} \qquad \ldots (15)$$

which is a pure integrator and a gain. This implies that feedback of the rate of climb to flap frequency with gain k_w is necessary for vertical speed control. The closed loop system can then be pre-connected to a controller with transfer function $D_1(s)$ and post-connected to an integrator to obtain the vertical position. The output from the integrator can then be fed back, forming an error signal ε_z with the demanded z-position z_{dmd}, as shown in Fig. 9.

In order to have good performance for both the step and ramp inputs, a proportional plus integral $P+I$ controller was used.

The exercise can be repeated for the horizontal axis control and an inner speed stabilisation loop with feedback gain k_u, a pre-connected $P+I$ controller and a post-connected integrator were included in the horizontal axis control system design in a similar fashion to that shown in Fig. 9. The final control system design for Concept 1 is shown in Fig. 10.

5.2 Control Concept 2

Figure (5) has shown that a variation in the phase φ between the pitch and flap attitudes of the wings results in a change in force magnitude and direction. In this design, phase φ is varied to change the force magnitude. The stroke plane tilt is used to control the direction of the resultant force. The pitch stabilised open loop system $G_2(s)$ is connected to a controller with transfer function $D_2(s)$ upstream and an integrator downstream as shown in Fig. 11. The linear transfer function $G_2(s)$ is given by

$$G_1(s) = \frac{w_b(s)}{\varphi_{dmd}(s)} = \frac{K_{fw}}{s} \qquad \ldots (16)$$

$D_2(s)$ controls the phase angle φ between the flap and pitch attitudes of the wings. Initially, a $P+I$ controller for each of the horizontal and the vertical axes were designed. However, it was found that there was a non-zero steady state error to a step input. This error can be minimised by the gains k_w of the speed stability loop, and k_p and T_i of the $P+I$ controller, but the ramp response posed a steady state tracking error. Improvement in the tracking performance can only be achieved at the expense of the poor damping in a step response.

In view of this, a PID controller was designed for the horizontal and vertical axis. The proportional and the speed stability gains as well as the integral time constant of the controller were designed to give good tracking performance while the differential component of the controller improves the stability of the step response.

Figures 12(a) and (b) show the horizontal position of the vehicle as a response to a step and ramp input respectively with two $P+I$ controllers with different gains and a PID controller. It can be seen that reducing the speed stability gain k_u improves the ramp response at the expense of the damping in the step response. The PID controller shows good results in both step and ramp response.

The final design for this flight control system concept is shown in Fig. 13.

5.3 Control Concept 3

In the previous controller design concepts, the pitch axis was stabilised simply by feeding back the pitch rate to the centre of gravity location with the gain k_q. In the present design concept, a more precise pitch attitude control is necessary as this determines the tilt of the fuselage for a more exact horizontal force control.

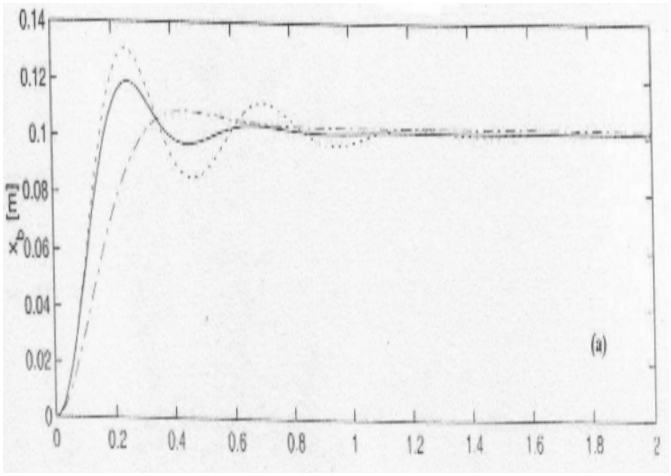

(a)

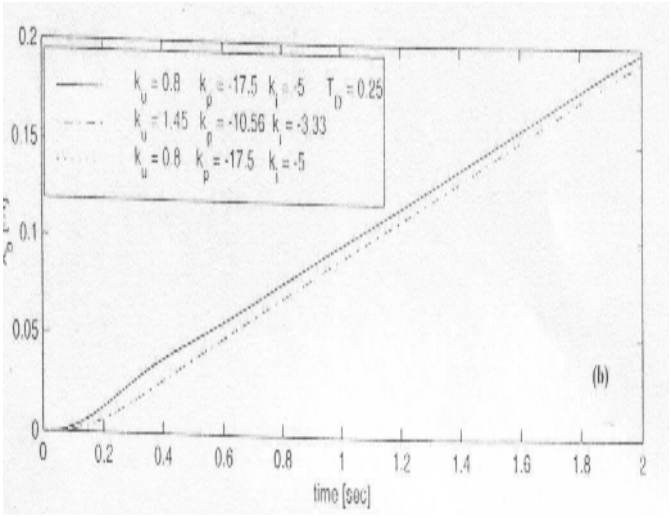

(b)

Figure 12. Response in control Concept 2, step input (a) and ramp input (b).

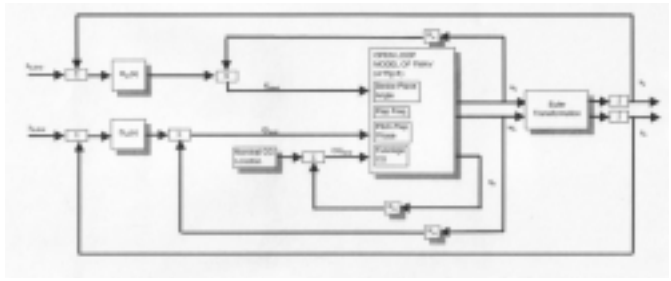

Figure 13. Flight control system for Concept 2.

Figure 14 shows the position demand system for the *x*-axis. The error signal ε_θ derived from the demanded and actual pitch attitude of the fuselage determines the CG location for the required fuselage tilt. It is fed to the pitch stabilised open loop system, $G_3(s)$ where

$$G_3(s) = \frac{\begin{bmatrix} u_b(s) \\ \theta(s) \end{bmatrix}}{\varphi_{dmd}(s)} = \frac{\begin{bmatrix} K_{\varphi u} \\ K_{\varphi\theta} \end{bmatrix}}{s} \quad \ldots (17)$$

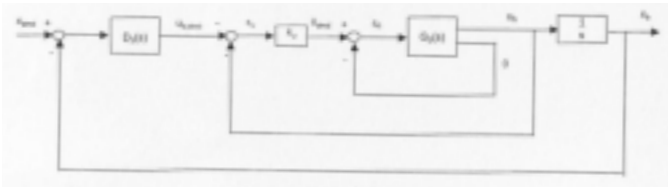

Figure 14. Horizontal position demand system.

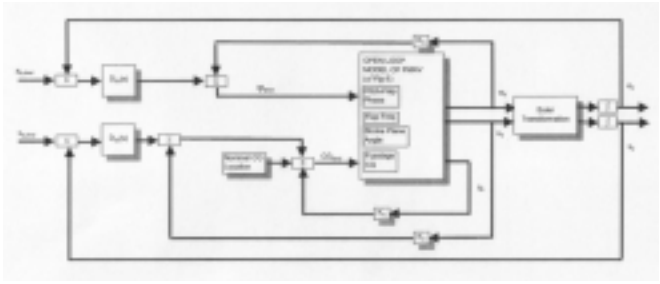

Figure 15. Flight control system for Concept 3.

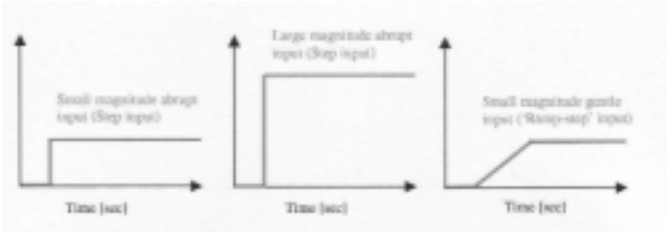

Figure 16. Types of inputs.

The output u_b is then connected to an integrator to obtain the *x*-position. The controller $D_3(s)$ is a PID controller for the same reason as mentioned earlier.

The vertical axis control loop is identical to that of the control Concept 2 as both employ the phase between flap and pitch attitude of the wing to modulate the force magnitude.

Figure 15 shows the final design of the control system for this concept.

6.0 COMPARISON OF DESIGN CONCEPTS

The three control system designs were tested using both step and ramp for the horizontal and vertical channels. Generally, step inputs may be considered as abrupt inputs while ramp inputs are gentler in nature. In this paper, the terms small amplitude abrupt input, large amplitude abrupt input and gentle input for the horizontal and vertical channels are defined in Fig. 16. It is acknowledged that small amplitude is subjective and for the vehicle of the size considered, a 30mm position change demand may be classified as large amplitude.

Figure 17 shows the typical response of the three flight control systems. The right hand column shows the vehicle position with respect to its initial position. The left hand column shows the variation of the horizontal control effector deflection $d\eta_x$, ratio of the control effector deflection from its trimmed state $d\eta_z/\eta_z$ and centre of gravity shift d_{1x}. For the vertical axis, the ratio is selected instead of the absolute change because different units (Hz for Concept 1 and degrees for Concept 2 and 3) are being used here. Table 4 shows the definition of the variables η_x and η_z.

Table 4
Control effectors in MAV

	η_x	η_y
Concept 1	κ[°]	n[Hz]
Concept 2	κ[°]	φ[°]
Concept 3	d_{1x}[mm]	φ[°]

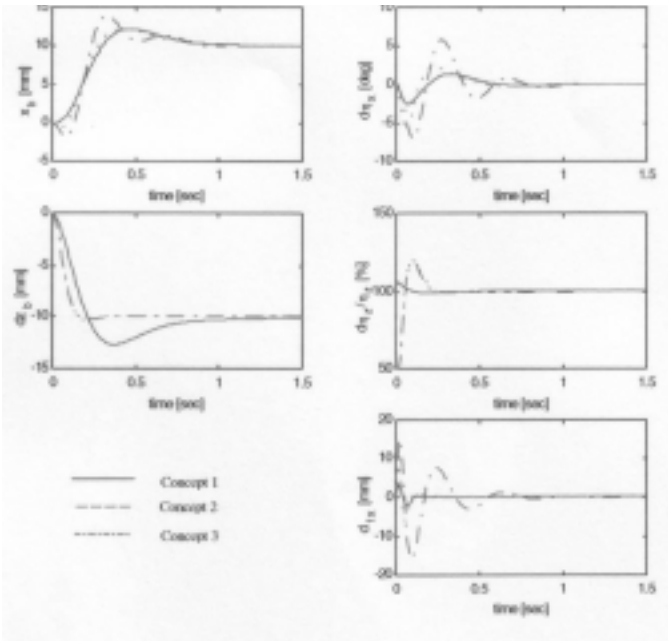

Figure 17. Typical response to simultaneous large amplitude abrupt inputs.

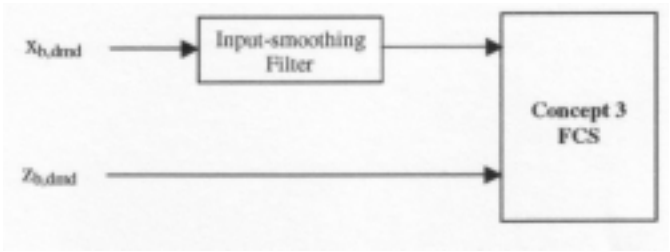

Figure 18. Connection of input-smoothing filter to FCS.

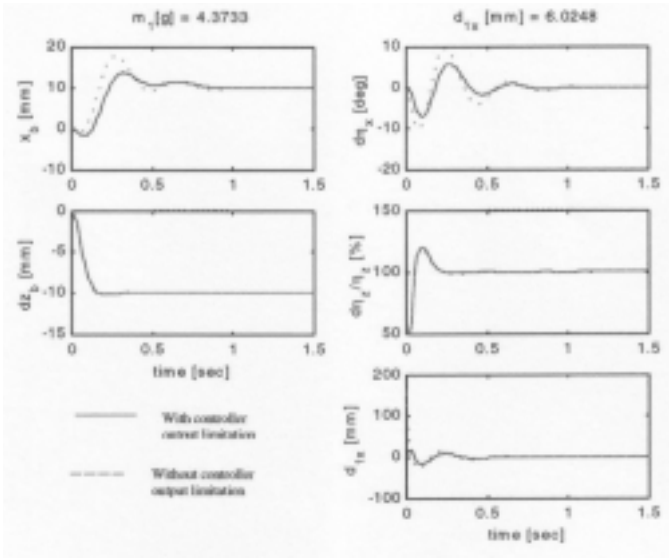

Figure 19. Effects of limiting controller output.

It can be seen from the typical responses shown in Fig. 17 that the control system designs result in well-behaved vehicle dynamics, provided that the control inputs are not excessively large. It was also found that abrupt inputs may cause saturation in the control system. The phase was seen to drop to 50% of the trim value. A built-in limiter with a 150% upper limit and 50% lower limit was included in the control system to prevent η_z from being reduced further.

Two criteria were used to compare the response of the three control designs, namely the range of CG shift required in the manoeuvres as well as the cross-axis response.

6.1 Shift in centre of gravity

It was seen in the simulations that the demanded shifts in the CG may exceed physical limits and the vehicle may not be controllable. If the fuselage is divided into two sections with equal mass and dimension, a 20mm shift of the CG will require one section to translate twice this distance relative to the other.

It can be seen in Fig. 17 that the shift in the centre of gravity in Concept 3 was greater than in the other two control concepts. This is because the fuselage has to pitch to direct the force accordingly and pitching of the fuselage is effected by the change in moment balance. The shift in the centre of gravity can be reduced by gentle inputs with smaller magnitudes, or when an input-smoothing filter is pre-connected to the controller as shown in Fig. 18. The variation of CG for Concept 3 with and without this input-smoothing filter is shown in Fig. 19. It was seen that by using an input-smoothing filter, the demand on fuselage tilt is reduced significantly, resulting in a more manageable demand on the CG shift. The overshoot in the horizontal position is also reduced.

6.2 Cross-axis response

The cross-axis response, or the response in one axis due to an input in the other, would have to be minimised for manoeuvres in enclosed spaces. If, for example a command to climb vertically behind a table results in excessive horizontal motion, the vehicle may bump into the table and thus result in loss of control.

It was found that Concept 1 has the best performance in this context for input in the vertical axis, as shown in Fig. 20. This is because a command to climb requires an increase in flap frequency, which changes the magnitude of the force but not the direction. As a result the vehicle moves vertically upwards since a control loop maintains pitch balance through CG shift and thus prevents the vehicle from accelerating forward.

In Concepts 2 and 3, a change in phase also results in a change in force direction, resulting in the vehicle accelerating forward before the stroke plane or fuselage can be tilted to counter this motion.

For large magnitude abrupt inputs in the horizontal axis, the performance of all three concepts was not as good. A forward acceleration is effected either by the tilt of the stroke plane or a tilt of the fuselage. This directs the force vector forward resulting in a reduced vertical component. The vehicle therefore loses altitude before the control system causes an increase in force magnitude. The simulation results shown in Fig. 21 show that a tilt in fuselage corrects the vertical displacement better than a tilt in the stroke plane.

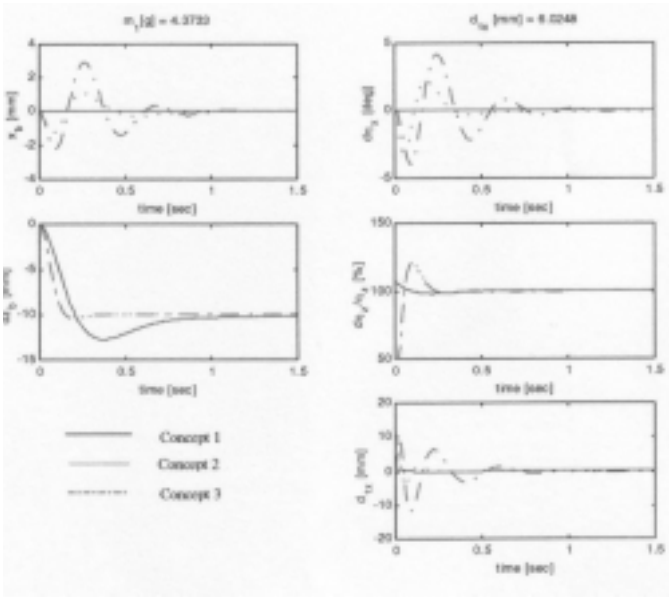

Figure 20. Comparison of cross-axis response vertical axis input.

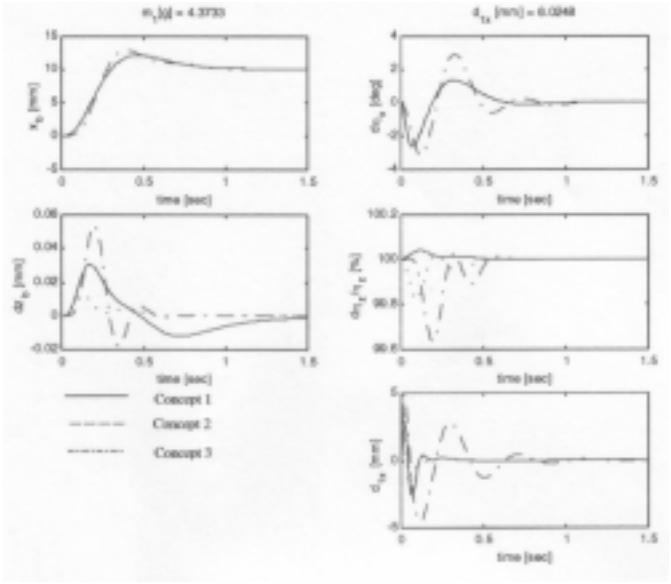

Figure 21. Comparison of cross-axis response horizontal axis input.

7.0 CONCLUSION

The foregoing describes the development of the equations of motion for a multi-body system representation of a flapping wing MAV. It was found that in order to avoid the computational problems associated with the simulation of a stiff system, the wing beat kinematics have to be time-averaged over each flap cycle. By so doing, the computational speed of the simulation was much improved without loss of fidelity as, by implication, the dynamic forces were also time-averaged.

Flight control systems were designed to meet three different control concepts using classical control methods. The controllers were developed and implemented with the aid of a non-linear time-averaged simulation model of the MAV. Although the control concepts evaluated are representative of many possible alternative control strategies for controlling an MAV at the hover, the investigation has exposed the design difficulties and limitations of a practical application.

Of particular interest, the concept of centre of gravity shift for stabilising the vehicle in pitch was successfully implemented. However, in manoeuvres with simultaneous large magnitude, abrupt inputs to both horizontal and vertical control axes, the demanded CG variations were too great. It was found that by limiting the output of the CG control loop, the CG shift can be reduced to an acceptable range, thereby enabling a feasible control strategy.

Cross-axis response, or cross coupling, was considered important, especially for operation in enclosed spaces. Clearly, a control mechanism for minimising cross coupling was necessary. The control of vertical position by variation of flap frequency was found superior to minimise cross axis response coupling. For abrupt inputs to the horizontal position control loop, the response lag resulting in transient loss of altitude could not be avoided completely. It was apparent that fuselage tilt for force direction control resulted in a marginally better performance in this context.

REFERENCES

1. McMasters, J.H. and Henderson, M.L. Low speed single element airfoil synthesis, *Technical Soaring*, 1980, **6**: pp 1-21.
2. Ellington, C.P. The aerodynamics of hovering insect flight I: The quasi-steady analysis, *Phil Trans R Soc Lond*, 1984, B 305, pp 1-15p
3. Ellington, C.P, The aerodynamics of hovering insect flight VI : Lift and power requirements, *Phil Trans R Soc Lond*, 1984, B 305, pp 145-181
4. Francis, R.H. and Cohen, J. The flow near a wing which starts suddenly from rest and then stalls, *Memo Aeronaut Res Comm*, 1933, **1561**.
5. Dickinson, M.H. and Lehmann, F.O., Sane S.P. Wing rotation and the aerodynamic basis of insect flight, *Science*, 1999, **284**, pp 1954-1960.
6. Dudle,y R. and Ellington, C.P. Mechanics of forward flight in bumble bees I: Kinematics and morphology, *J Exp Biol*, 1990, **48**, pp 19-52.
7. Dudley, R. and Ellington, C.P. Mechanics of forward flight in bumble bees II : Quasi-steady lift and power requirements, *J Exp Biol*, 1990, **148**, pp 53-58.
8. Tennekes, H. *The Simple Science of Flight*, 1997, MIT Press.
9. Zbikowski, R. Flapping wing autonomous micro air vehicles: Research programme outline, 1999, Paper 38, 14th International Conference, Unmanned Aerial Vehicles, April 1999, Bristol, UK.
10. DeLaurier, J.D. and Harris J.M. A study of mechanical flapping wing flight, *Aeronaut J*, Oct 1993, **97**, (968), pp 277-286.
11. Gad-el-Hak, M. Micro air vehicles: Can they be controlled better?, *J Aircr*, 2001, **38**, (3), pp 419-429.
12. Michelson, R.C. and Reece S. Update on flapping wing micro air vehicle research: Ongoing work to develop a flapping wing, crawling 'entomopter', 1998, Paper 30, 13th International Conference of Unmanned Aerial Vehicles, Bristol, UK.
13. Ellington, C.P. The aerodynamics of hovering insect flight III : Kinematics, *Phil Trans R Soc Lond*, 1984, B305, pp 41-78.
14. Willmott, A.P. and Ellington, C.P. Measuring the angle of attack of beating insect wings: robust three-dimensional reconstruction from two-dimensional images, *J Exp Biol*, 1997, **200**, pp 2693-2704.
15. Willmot, A.P. and Ellington, C.P. The mechanics of flight in the hawkmoth Manduca sexta I: Kinematics of hovering and forward flight, *J Exp Biol*, 1997, **200**, pp 2705-2722.
16. Lehmann, F.O. and Dickinson, M.H. The control of wing kinematics and flight forces in fruit flies (Drosophila spp), *J Exp Biol*, 1998, **201**, pp 385-401.
17. Tobalske, B.W., Peacock, W.L. and Dial, K.P. , Kinematics of flap-bounding flight in the zebra finch over a wide range of speeds, *J Exp Biol*, 1999, **202**, pp 1725-1739.
18. Pennycuick, C.J., Hedenstrom, A. and Rosen, M. Horizontal flight of a swallow (Hirundo rustica) observed in a wind tunnel, with a new method for directly measuring mechanical power, *J Exp Biol*, 2000, **203**, pp 1755-1765.
19. Smith, M.J.C., Wilkin, P.J. and Williams, M.H., The advantages of an unsteady panel method in modeling the aerodynamic forces on rigid flapping wings, *J Exp Biol*, 1996, **199**, pp 1073-1083.

20. VEST, M.S. Unsteady Aerodynamics and Propulsive Characteristics of Flapping Wings with Applications to Avian Flight, Doctoral dissertation, 1996, San Diego State University and University of California, San Diego.
21. LIU, H. and KAWACHI, K. A numerical study of insect flight, *J Comp Physics*, 1998, **146**, pp 124-156, Article No CP986019.
22. VAN DEN BERG, C. and ELLINGTON, C.P. The vortex wake of a hovering model hawkmoth, *Phil Trans R Soc Lond*, 1997, **352**, pp 317-328.
23. BILO, D., LAUCK, A. and NACHTIGALL, W. Measurements of linear body accelerations and calculations of instantaneous aerodynamic lift and thrust in a pigeon flying in a wind tunnel, *Biona Report 3 — Bird Flight - Vogelflug*, NACHTIGALL, W., (Ed), 1985, Gustav Fischer, Stuttgart.
24. FEJTEK, I. and NEHERA, J. Experimental study of flapping wing lift and propulsion, *Aeronaut J*, 1980, **84**, pp 28-33
25. VEST, M.S. and KATZ, J. Aerodynamic study of a flapping wing micro-UAV, 1999, AIAA99-0994, 37th AIAA Aerospace Sciences Meeting and Exhibit, Reno, NV, USA.
26. DICKINSON, M. The effects of wing rotation on unsteady aerodynamic performance at low Reynolds numbers, *J Exp Biol*, 1994, **192**, pp 179-206.
27. SANE, S.P. and DICKINSON, M.H. The control of flight force by a flapping wing: lift and drag production, *J Exp Biol*, 2001, **204**, pp 2607-2626.
28. LOH, K.H. An Investigation into the Hovering Flight Dynamics and Control of a Flapping Wing Micro Air Vehicle, 2003, PhD thesis, College of Aeronautics, Cranfield University.
29. ELLINGTON, C.P. The novel aerodynamics of insect based flying machines, 1999, Paper 37, 14th International Conference of Unmanned Aerial Vehicles, Bristol, UK
30. ROBERTSON, R.M. and JOHNSON, A.G. Collision avoidance of flying locusts: steering torques and behaviour, *J Exp Biol*, 1993, **183**, pp 35-60.
31. RASHID, T. The Flight Dynamics of a Full-Scale Ornithopter, 1995, MASc thesis, University of Toronto, Institute of Aerospace Studies.
32. DENG, X., SCHENATO, L. and SASTRY, S. Hovering flight control of a micromechanical flying insect, 2001, Proceedings of the 40th IEEE Conference on Decision and Control, Orlando, Florida, USA.
33. SCHENATO, L., DENG, X. and WU, W.C. Sastry S. Flight control system for a micromechanical flying insect: Architecture and implementation, 2001, Proceedings of the 2001 IEEE Conference on Robotics & Automation, pp 1641-1646, Seoul, South Korea.
34. SCHENATO L., DENG, X. ands WU, W.C. Sastry S, Virtual insect flight simulator (VIFS): A software testbed for insect flight, 2001, p3885-3892, Proceedings of the 2001 IEEE Conference on Robotics & Automation, Seoul, South Korea.
35. MCFARLAND M.W. *The Papers of Wilbur and Orville Wright — Volume One 1899-1905*, 1953, McGraw-Hill.